

CRUCIFORM BIAXIAL FLEXURAL TESTING OF POLYGRANULAR NUCLEAR GRAPHITE

Dong Liu¹, Mahmoud Mostafavi², T. James Marrow², David J. Smith³ and Peter E. J. Flewitt^{1,4}

¹ Interface Analysis Centre, School of Physics, University of Bristol, UK

² Department of Materials and Oxford Martin School, University of Oxford, UK

³ Department of Mechanical Engineering, University of Bristol, UK

⁴ HH Wills Physics Laboratory, School of Physics, University of Bristol, UK

ABSTRACT

The effect of stress state on the flexural strength of a quasi-brittle material is explored using reactor core Gilsocarbon graphite. The test geometry adopted has a ‘five-point’ bending configuration, i.e. a cruciform-shaped specimen that creates a tensile biaxial stress on the surface. This allows the effect of changing the biaxial ratio on the load-displacement and fracture characteristics to be considered. An acoustic emission (AE) technique has been applied to monitor and identify the occurrence of acoustic events and their locations in specimens loaded either monotonically to failure or via several progressively increasing load-unloading cycles. It was found that the fracture path changes with biaxial ratio. AE events occurred from low load in all loading modes, and increased progressively with the increase of applied load. The total number of AE events and the sum of the cascade energy from the AE measurements were similar for specimens fractured at the same load under a particular loading condition.

INTRODUCTION

Gilsocarbon graphite is used as the neutron moderator in the advanced gas-cooled reactors (AGRs) in the UK. It also acts as a structural component providing channels for the coolant gas, fuel, control rods and safety shutdown devices in these reactors (Rose et al. 1982)(Moskovic et al. 2014). In addition, isotropic and near-isotropic nuclear-grade graphite is a candidate material for the nuclear moderator and major structural components in some designs of Generation IV advanced reactors. For this reason, the structural integrity assessment of nuclear graphite components in terms of deformation and fracture is an essential element of reactor design and operation (Hodgkins et al. 2010)(Liu et al. 2015)(Yaghi et al. 2004). In addition to self-weight load, graphite bricks are subject to complex loading from shrinkage and thermal stresses, as well as restraint loads and possible seismic impact loads over the life of the reactor (Kelly 1982). Therefore, an understanding of the properties of the graphite under complex loading conditions is important for high confidence in integrity assessments (Bradford et al. 2008)(Sato et al. 1986).

As with many quasi-brittle polycrystalline materials, the failure load depends on the loading configuration, component geometry and size. The present work investigates the deformation and fracture of Gilsocarbon graphite under different biaxial loading conditions. Typically, Gilsocarbon graphite is stronger in bending (~30 MPa) than tension (~20 MPa) and stronger in compression (~70 MPa) than bending (Brocklehurst et al. 1974). Various approaches have been adopted to measure the biaxial strength of materials, for example, axial loading combined with internal pressure on tubular specimens, ring-on-ring tests on thin plates and biaxial tension/compression on cruciform specimens. Large tests (cm-scale) (Burchell et al. 2007) of extruded near-isotropic medium-grain size nuclear graphite (grade H-451) subject to uniaxial tension or compression and internal pressure showed that there is an approximate 20% reduction in flexural strength compared to uniaxial loading. Mostafavi et al (Mostafavi et al. 2013) tested Gilsocarbon graphite under equi-biaxial loading using a ring-on-ring configuration and found an approximately 20% strength reduction relative to the uniaxial flexural strength; similar results have been reported by testing tubular isotropic

nuclear graphite (the fine-grained 2020 grade of Stackpole Carbon Company and the coarse-grain PGX of Union Carbide Corp) under axial loading and internal or external pressure (Ho et al. 1983).

Acoustic emission (AE) has been used in several studies to detect the evolution of damage in graphite under deformation (Burchell et al. 1986)(Neighbour et al. 1992). AE characterises the transient elastic mechanical wave generated by the burst of energy from localised sources within a stressed material (Pollock 1973)(Neighbour et al. 1995). Depending on the type of brittle fracture, the amplitude, frequency and waveform of the acoustic events vary. For instance, tensile fracture tends to generate events with higher amplitude than shear; micro-cracks generate a larger number of events with small amplitude while macro-crack growth tends to produce fewer events but with a larger amplitude. The analysis of these events can indicate the amount of damage, the form of cracking and if more sensors are adopted, the location of the source can be identified (Carpinteri et al. 2007).

This paper presents the results obtained from a range of biaxial tests conducted on Gilsocarbon graphite using a cruciform test specimen subjected to ‘five-point’ loading. Acoustic emission has been used to detect the occurrence and location of damage during loading. The results are discussed in the context of the degree of biaxiality with respect to the failure strength, crack initiation and propagation path.

EXPERIMENTS

The material studied was unirradiated Gilsocarbon graphite, which was a near-isotropic (1 : 1.1) moulded graphite, extracted from stock AGR reactor core bricks provided by EDF Energy Ltd. The filler coke particles, Gilsocarbon, produced by calcination of Gilsonite, had a diameter of around 0.5 mm. Cruciform specimens (150 mm x 150 mm x 20 mm) were loaded using a ‘five-point’ bending configuration (Fig. 1a). There was a single point of contact using an aluminum sphere of diameter 10 mm at the centre and top surface of the cruciform specimen, with line contacts using aluminum rollers of diameter 10 mm on the bottom surface at each of the arms. The direction of the loading relative to the specimens are shown by arrows in Fig. 1a. The loading system was made from aluminum alloy (6000 Series); there were three positions where the rollers were placed as shown in Fig. 1b by dashed lines. By moving the roller between positions 1 to 3, with increasing distance from the centre of the specimen (50 mm, 60 mm and 70 mm), the biaxial ratio, α , was changed (Fig. 1b). When rollers on one pair of arms were at position 3 and the others at position 2, the loading condition was described as ‘3-2’. The radius of the transition between the arms was designed to be 10 mm by finite element modelling to ensure that the highest stress was at the centre of the specimen under equi-biaxial bending. All the tests were undertaken using an Instron MJ6272 27 kN loading machine with displacement control at a cross-head speed of 0.02 mm/min. During each test, a pointer was used to align the specimen prior to loading.

Four resonance transducers (Pancom model P15 with frequency 150 kHz) were attached to the surface via an ultrasonic couplant with electrical tape; each transducer had a diameter of 20 mm and was placed 60 mm from the centre of the specimen along each arm. Using a pencil lead break (which corresponds to a Hsu-Nielsen source) located between the sensors, the velocity of sound was determined to be $\sim 2700 \text{ m}\cdot\text{s}^{-1}$ (velocity = distance / delta time). The threshold for recording AE events was set at 40 dB.

Four sets of experiments were undertaken:

- (i) Calibration of the loading configuration using a strain-gauged Perspex specimen for loading conditions 3-3, 3-2, 3-1 and 3-0 (and without AE measurements) (Fig. 2a); Four uniaxial strain gauges (EA-06-240LZ-120/E) were attached by M-Bond 200 to the top surface of the Perspex specimen 25 mm away from the centre along the loading arms ;
- (ii) Crushing tests, applied to the Gilsocarbon cruciform tests, were used to identify AE events from the loading contacts during loading;

- (iii) Fracture tests for cruciform specimens with the 3-2, 3-3 and 3-0 loading conditions and with AE measurements;
- (iv) Fracture tests of a uniaxial flexure beam, i.e. with a pair of arms removed from a cruciform specimen (Figs. 2b and 2c). With the roller support at position 3, a pointer was used to align the beam to the centre of the loading ball. Two AE sensors were then attached, each 60 mm from the centre of the specimen.

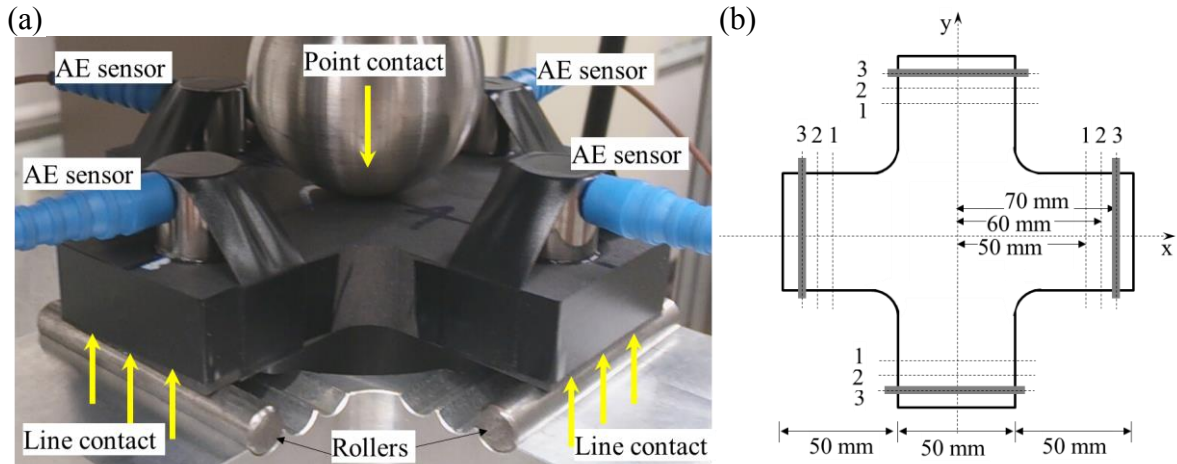


Fig. 1 (a) The ‘five-point’ loading system showing 3-3 loading condition: the ‘five-point’ loading consisted of one point contact by an aluminum ball (10 mm dia.) at the centre and top surface of the specimen, and four line contacts provided by four aluminum rollers (10 mm dia.); one at each arm. Four AE sensors held in place by electrical tape and ultrasound couplant; (b) the dimension of the specimen, numbering and the roller positions at each arm; the thickness of the specimen was 20 mm. Each dashed line at the end of arms represents a position where a roller was placed. The diagram shows a typical 3-3 loading condition with four rollers being placed at the outer most position of each arm.

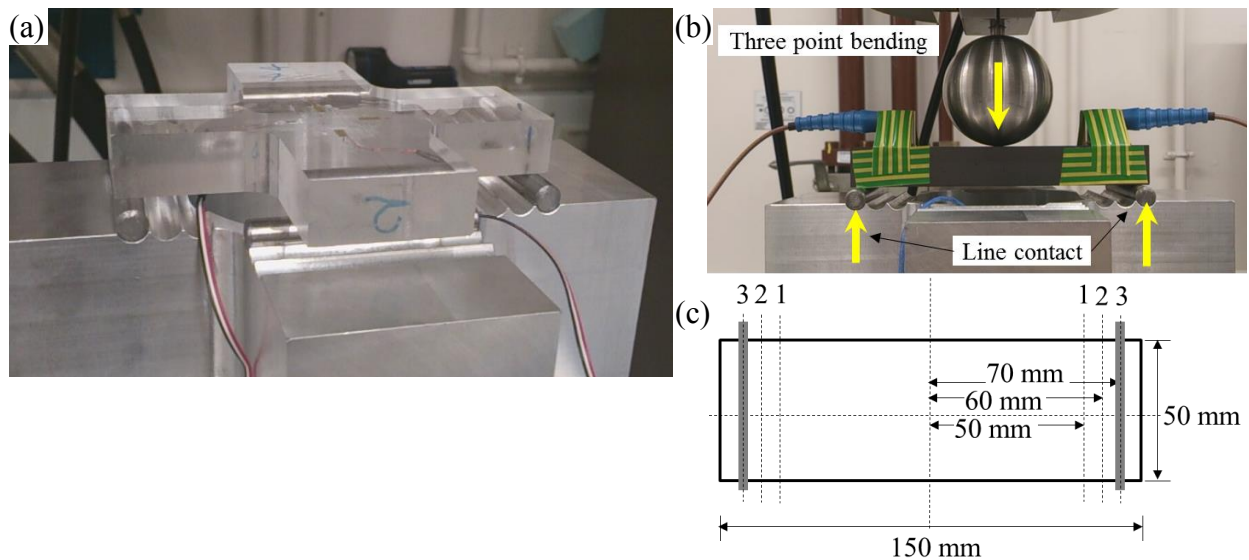


Fig. 2 (a) Perspex calibration specimen on the loading jig showing the four strain gauges on the tensile surface along the centerline of arms (each strain gauge was 25 mm away from the specimen centre); (b) the ‘three-point’ loading of a beam (with a pair of arms removed) consisted of a single point contact on the top surface and two line contacts from the supporting rollers, and (c) the 3-0 supporting span during loading.

RESULTS AND DISCUSSION

Calibrations

Example data obtained from the calibration test on Perspex specimens are shown in Fig 3, as the load was cycled. The Perspex tests demonstrated that the strains in each arm was uniform for 3-3 loading (i.e. the loading system provided the intended loading). For 3-2 loading, the two pairing strain gauges showed consistent values with each other. Based on these calibration experiments the loading conditions adopted for the Gilsocarbon graphite specimens were 3-3, 3-0 and 3-2. These gave equi-biaxial, uniaxial and an approximate 6:7 biaxial ratio (this biaxial ratio of the stresses at the centre of the specimen was estimated by calculating the length of loading arms - for instance, the loading arm length was 70 mm and 60 mm under 3-2 loading condition, the biaxial ratio under that condition was therefore considered to be 6:7). During the crushing tests, the total number of AE events observed was typically 10% to 15% of that detected in the fracture tests, with amplitudes below 55 to 60 dB.

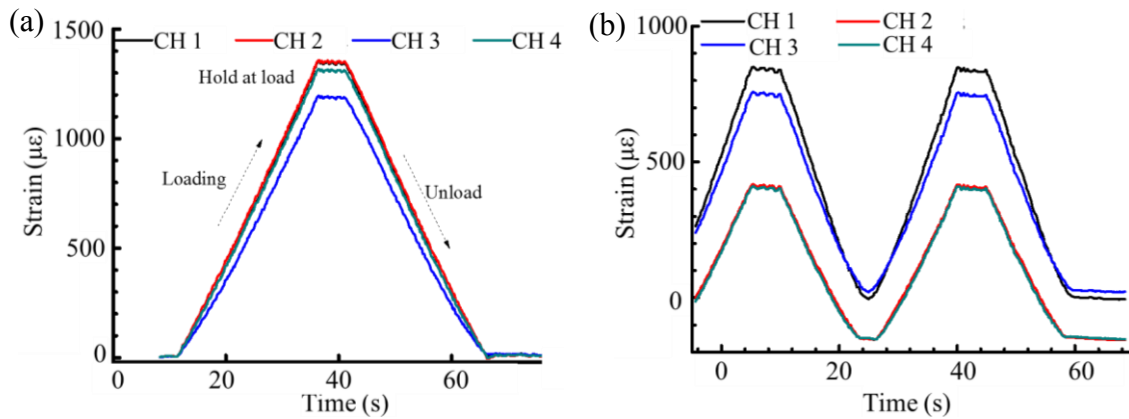


Fig. 3 Strains from the four strain gauges, Channel 1 to 4 (CH 1, CH2, CH3 and CH4) on a Perspex specimen under (a) 3-3 loading condition and (b) 3-2 showing the similar strains from gauges at similar locations.

Maximum load to fracture and fracture path

The test conditions and failure loads for the cruciform graphite specimens are summarised in Table I. Two specimens were tested under each loading condition: one was loaded directly to failure and the other was loaded through several displacement-controlled cycles. The uniaxial flexural beam was tested under loading-unloading cycles with rollers at support position 3 ('Beam 3-0' in Table I). Data for the 3-3 and 3-0 tests showed that the maximum load at fracture was unaffected by the loading sequence.

Table I Experimental and predicted maximum loads (kN) at fracture for each loading condition.

Loading conditions (Biaxiality Ratio, α)	3-3 ($\alpha=1:1$)	3-0 ($\alpha=1:0$)	3-2 ($\alpha=6:7$)	Beam 3-0 ($\alpha=1:0$)
Single load to failure	-5.4	-4.2	-5.8	-
Cyclic load to failure	-5.3	-4.1	-6.8	-2.6

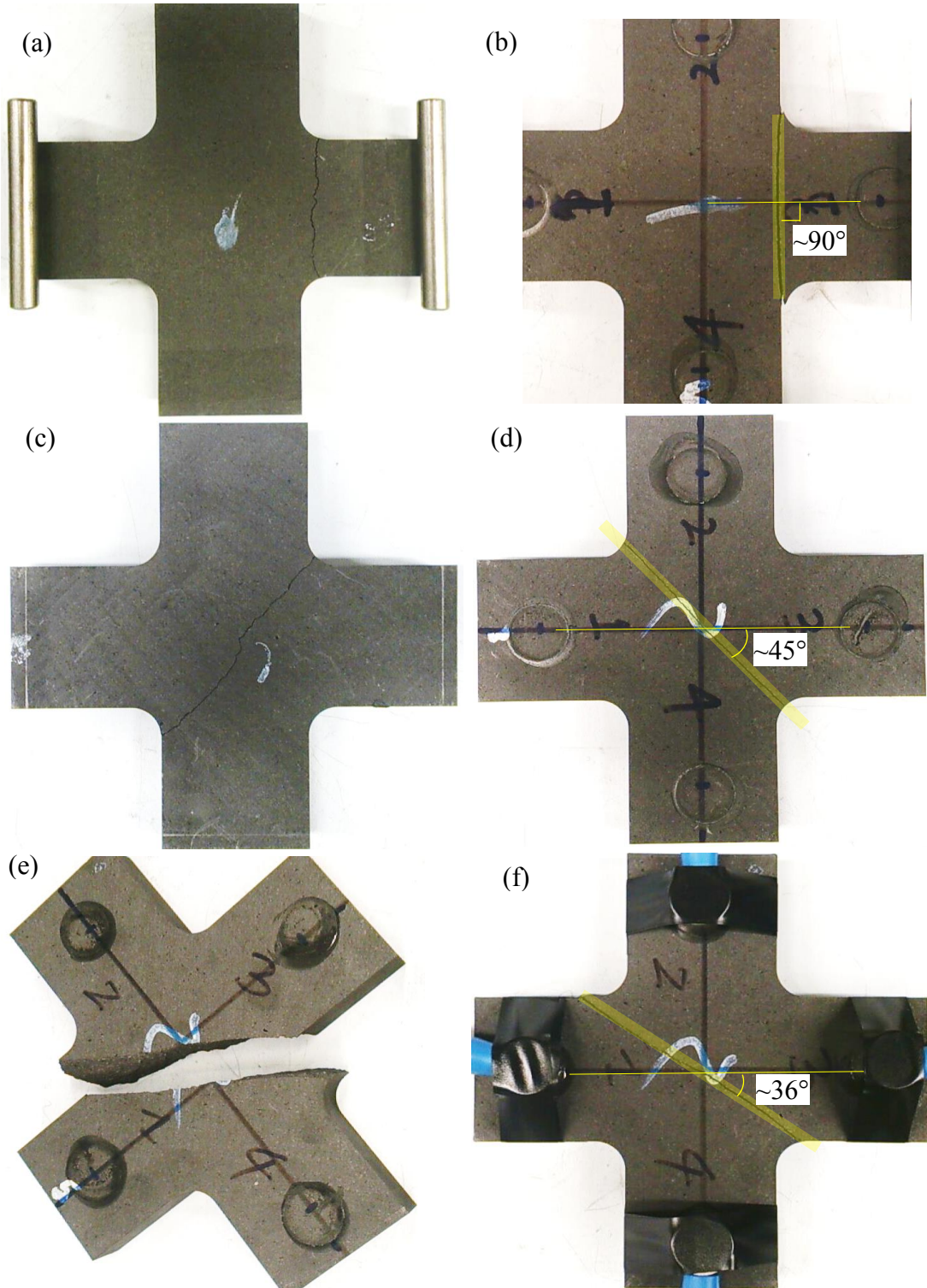


Fig. 4 The fracture path for the Gilsocarbon specimens tested at three conditions: (a) and (b) are the tensile surface and compressive surface of 3-0 condition (the rollers are placed on the specimen to show the supporting positions); (c) and (d) are the tensile surface and compressive surface of 3-3 condition; (e) shows the deflected crack path through the thickness of the specimen fractured under 3-2 condition and (f) is the compressive surface of the 3-2 specimen.

The fracture path of specimens subjected to different biaxial ratios was found to vary (Fig. 4). For the 3-0 condition, final fracture was located at the smallest section across the width of one of the supported arms (Figs. 4a and 4b). The fracture path was tortuous on the tensile surface (Fig. 4a), but was straight and smooth after propagating to the compressive side (Fig. 4b). For specimens fractured under the 3-3 condition, the fracture path was about 45° across the central area, between the corners of the arms. Similarly to the 3-0 condition, the fracture path on the tensile surface was tortuous (Fig. 4c), and straight on the compressive side. For the 3-2 condition, the fracture path follows a smaller angle (about 36°) (Fig. 4e), but was otherwise similar to the other specimens (Fig. 4f). For each pair of specimens tested at the same loading condition, the angle of the crack path differed by less than 2°. The beam specimen (with the arms removed) fractured in the middle of the span.

The differences in final failure load between replicate specimens were small (less than 4% for the 3-0 and 3-3 specimens; and ~16% for the 3-2 specimens), and the maximum load increases with increased biaxiality. Sato et al (Sato et al. 1987) proposed that for the near-isotropic graphite (IG-11) under a multi-axial stress state in which tensile stresses are predominant, the maximum principal stress can be invoked as the failure criterion. A linear-elastic finite element calculation was undertaken in the current study to find the maximum load at failure using experimental uniaxial strength data reported by Mostafavi (Mostafavi et al. 2013). The predicted mean fracture load for the 3-0 beam was 2.65 kN. The geometrical constraint of the extra arms in a cruciform specimen increases the stiffness, leading to a higher failure load compared with the plain beam and also changed the fracture path.

Fracture process and acoustic events

Significant acoustic emission events did not commence at the beginning of loading, as evidenced in the example for monotonic loading under the 3-3 condition (Fig. 5a). The AE results (amplitude of the acoustic signal and applied load as a function of time - data collected from all four channels) for the 3-3 specimen under cycle load to failure are presented in Fig. 5b (in the AE plots, 1 eu = 1 E⁻¹⁸ Js at 10 kW preamplifier input => 1 E⁻¹⁴V²s; amplitude is in dB, 0 dB = 1 μV at preamplifier input). In general, continuous AE signals occurred when the applied load exceeded about 30% to 40% of the maximum load; the final rapid failure resulted in a sudden increase in counts, energy and amplitude of the AE events (Figs. 5a and 5c). In specimens that were subjected to load-unload cycles before failure, the AE events occurred predominantly during loading.

The total number of acoustic events and the sum energy recorded during the entire loading process are listed in Table II. The data for the 3-3 and 3-0 tests show the total number of AE events were similar for specimens fractured at the similar loads under the same loading condition. The two specimens tested under 3-2 condition show a difference in terms of the total number of AE events; the maximum load to fracture for these two specimens had a 16% difference (~1 kN) compared with the other two groups (3-0 and 3-3). This difference was also reflected in the total energy to fracture, Table II.

Table II Summary of acoustic emission observations.

Loading conditions	3-3	3-0	3-2	Beam 3-0
Total number of events				
Single load to failure	~1340	~2290	~1600	-
Cycle load to failure	~1330	~2220	~2040	~900 (two sensors)
Sum cascade energy (eu x 10³)				
Single load to failure	69.7	113.8	96.8	-
Cycle load to failure	58.8	95.8	128.9	38.5
Difference (%)	15.6	15.8	25.5	-

The AE results confirmed that Gilsocarbon graphite does not fracture abruptly. There appeared to be an accumulation of micro-events prior to the final failure. This is characteristic of quasi-brittle materials. Indeed, this near-isotropic polygranular graphite has microstructural features similar to other aggregate and porous materials such as needle-coke polygranular graphites (Moskovic et al. 2013) and concrete (Bazant 1997)(Schlangen et al. 2009). The AE events recorded during loading were consistent with the presence of distributed micro-cracks, which form in the process zones developed before the peak load. It has been observed in the present work as well as by other workers (Brocklehurst et al. 1974) that the post-peak macro-cracking was irregular and led to progressive rather than prompt failure.

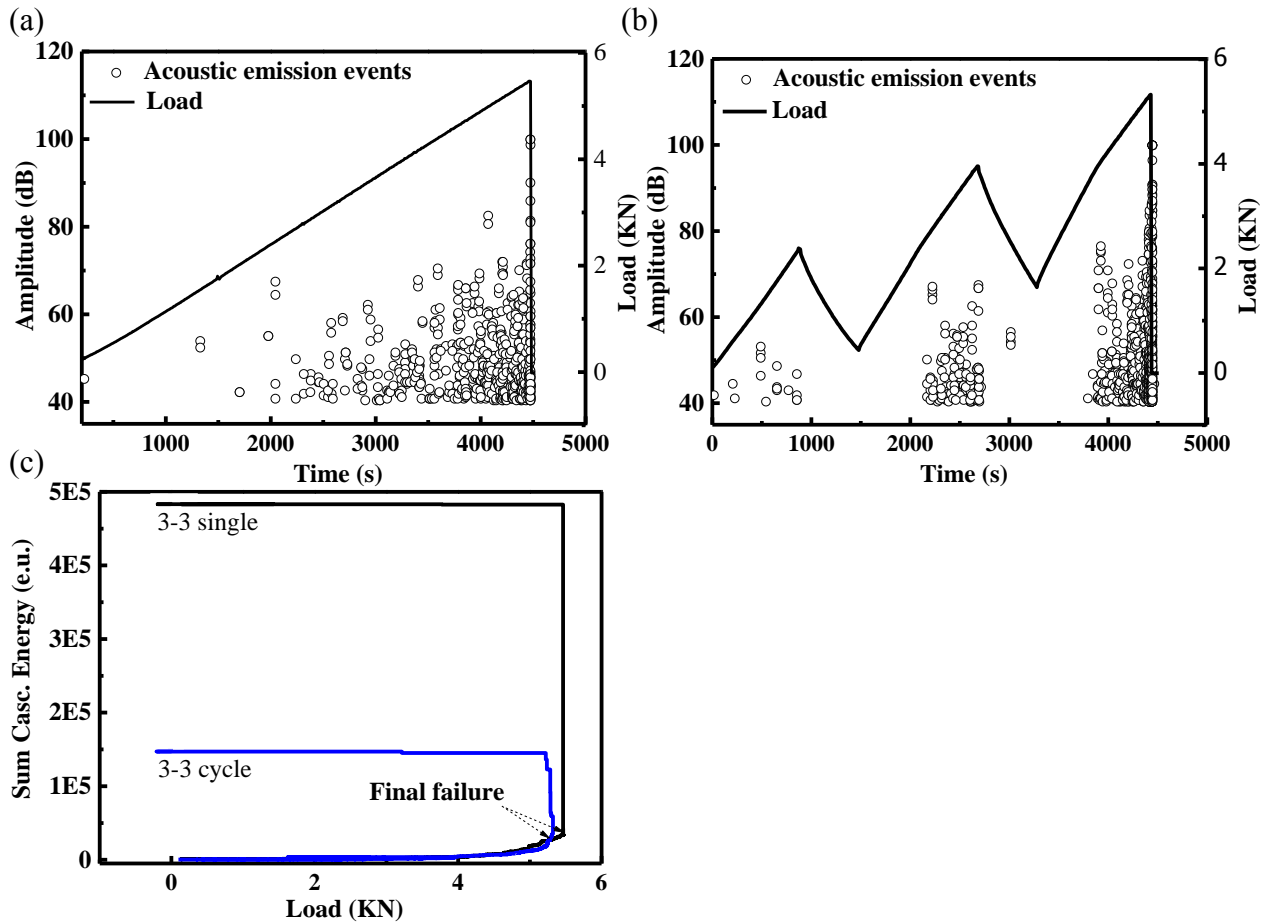


Fig. 5 Acoustic emission results for (a) 3-3 monotonic loading and (b) 3-3 cycle loading; (c) sum cascade energy as a function of load for 3-3 single and 3-3 cycle.

CONCLUDING COMMENTS

A cruciform geometry test specimen allows the role of biaxial loading to be explored for reactor core graphite. The current experimental arrangement demonstrates that different biaxial ratios may be applied to cruciform specimen, and the load-displacement behaviour monitored. It may be concluded that:

- (i) The fracture path changes with biaxial ratio;
- (ii) The total number of AE events increases with increased maximum load and those with higher energy become more frequent at higher load; events with the highest amplitude occurred at or near to the final fracture of the specimen.

ACKNOWLEDGEMENTS

The authors acknowledge financial support from EPSRC grant number EP/J019801/1 (Bristol): QUBE: QUasi-Brittle fracture: a 3D Experimentally-validated approach. PEJF thanks Wolfson College, Oxford, for facilitating the collaboration. D. J. Smith is grateful for the support provided by the Royal Academy of Engineering, EDF-Energy, Rolls Royce and the University of Bristol.

REFERENCES

- Bazant, Z.P. (1997). "Scaling of Quasibrittle Fracture: Asymptotic Analysis." *International Journal of Fracture* 83(1): 19–40.
- Bradford, M.R. and Steer, A.G. (2008). "A Structurally-Based Model of Irradiated Graphite Properties." *Journal of Nuclear Materials* 381(1-2): 137–44.
- Brocklehurst, J.E. and Darby, M.I. (1974). "Concerning the Fracture of Graphite under Different Test Conditions." *Materials Science and Engineering: A* 16(1-2): 91–106.
- Burchell, T., Yahr, T. and Battiste, R. (2007). "Modeling the Multiaxial Strength of H-451 Nuclear Grade Graphite." *Carbon* 45(13): 2570–83.
- Burchell, T.D., Rose, A.P.G. and McEnaney, B. (1986). "Acoustic Emission from Irradiated Nuclear Graphite." *Journal of Nuclear Materials* 140(1): 11–18.
- Carpinteri, A., Lacidogna, G. and Pugno, N. (2007). "Structural Damage Diagnosis and Life-Time Assessment by Acoustic Emission Monitoring." *Engineering Fracture Mechanics* 74(1-2): 273–89.
- Ho, F.H.; Vollman, R.E.; Yu, H. (1983). "Biaxial Failure Surfaces of 2020 and PGX Graphites." In *Transactions of the 7. International Conference on Structural Mechanics in Reactor Technology. Vol. L, ,* 127–34.
- Hodgkins, A., Marrow, T.J., Wootton, M.R., Moskovic, R. and Flewitt, P.E.J. (2010). "Fracture Behaviour of Radiolytically Oxidised Reactor Core Graphites: A View." *Material Science and Technology* 26(8): 899–907.
- Kelly, B.T. (1982). "Graphite-the Most Fascinating Nuclear Material." *Carbon* 20(1): 3–11.
- Liu, D., Nakhodchi, S., Heard, P. and Flewitt, P.E.J. (2015). "Small-Scale Approaches to Evaluate the Mechanical Properties of Quasi-Brittle Reactor Core Graphite." *Graphite Testing for Nuclear Applications: The Significance of Test Specimen Volume and Geometry and the Statistical Significance of Test Specimen Population* STP1578(Nassia Tzelepi and Mark Carroll, Eds.): 1–21.
- Moskovic, R., Flewitt, P.E.J., Schlangen, E., Smith, G., Crocker, A.G., Hodgkins, A., Heard, P. and Wootton, M.R. (2014). "Understanding Fracture Behaviour of PGA Reactor Core Graphite: Perspective." *Material Science and Technology* 30(2): 129–45.
- Moskovic, R., Heard, P.J., Flewitt, P.E.J. and Wootton, M.R. (2013). "Overview of Strength, Crack Propagation and Fracture of Nuclear Reactor Moderator Graphite." *Nuclear Engineering and Design* 263(0): 431–42.
- Mostafavi, M., McDonald, S.A., Çetinel, H., Mummery, P.M. and Marrow, T.J. (2013). "Flexural Strength and Defect Behaviour of Polygranular Graphite under Different States of Stress." *Carbon* 59(0): 325–36.
- Neighbour, G.B. and McEnaney, B. (1995). "An Investigation of Acoustic Emission from an Irradiated Nuclear Graphite." *Journal of Nuclear Materials* 223(3): 305–11.
- Neighbour, G.B., McEnaney, B. and Phillips, M. (1992). "Acoustic Emission Responses from Cyclic Loading of a Nuclear Graphite." *Carbon* 30(3): 359–63.
- Pollock, A.A. (1973). "Acoustic Emission - 2." *Non-Destructive Testing* 6(5): 264–69.
- Rose, A.P.G. and Tucker, M.O. (1982). "A Fracture Criterion for Nuclear Graphite." *Journal of Nuclear Materials* 110(2-3): 186–95.

- Sato, S., Awaji, H., Kawamata, K., Kurumada, A. and Oku, T. (1986). "Fracture Criteria of Reactor Graphite under Multi-Axial Stress State." *Journal of the Atomic Energy Society of Japan / Atomic Energy Society of Japan* 28(12): 1172–79.
- Sato, S., Awaji, H., Kawamata, K., Kurumada, A. and Oku, T. (1987). "Fracture Criteria of Reactor Graphite under Multiaxial Stesses." *Nuclear Engineering and Design* 103(3): 291–300.
- Schlagen, E. and Qian, Z. (2009). "3D Modelling of Fracture in Cement-Based Materials." *Journal of Multiscale Modelling* 01(02): 245–61.
- Yaghi, A.Y., Hyde, T.H., Becker, A.A. and Walker, G. (2004). *The Integrity of Graphite Blocks in Nuclear Reactors*. University of Nottingham Report. GRA/AHY/040806.